# Defects in cell spreading and ERK1/2 activation in fibroblasts with lamin A/C mutations

Lindsay J. Emerson, Mark R. Holt, Matthew A. Wheeler, Manfred Wehnert, Maddy Parsons, Juliet A. Ellis

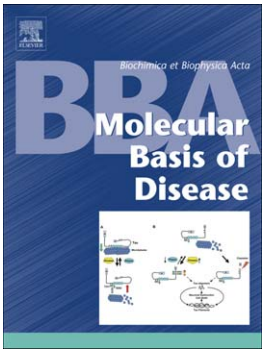


# Defects in cell spreading and ERK1/2 activation in fibroblasts with lamin A/C mutations

Lindsay J. Emerson, Mark R. Holt, Matthew A. Wheeler, Manfred Wehnert, Maddy Parsons, Juliet A. Ellis

PII: S0925-4439(09)00132-X
DOI: doi:10.1016/j.bbadis.2009.05.007
Reference: BBADIS 62962

To appear in: *BBA - Molecular Basis of Disease*

Received date: 30 March 2009
Revised date: 5 May 2009
Accepted date: 13 May 2009

Please cite this article as: Lindsay J. Emerson, Mark R. Holt, Matthew A. Wheeler, Manfred Wehnert, Maddy Parsons, Juliet A. Ellis, Defects in cell spreading and ERK1/2 activation in fibroblasts with lamin A/C mutations, *BBA - Molecular Basis of Disease* (2009), doi:10.1016/j.bbadis.2009.05.007

# Defects in cell spreading and ERK1/2 activation in fibroblasts with lamin A/C mutations

[#1]Lindsay J. Emerson, [#1]Mark R. Holt, [1]Matthew A. Wheeler, [2]Manfred Wehnert, [1]Maddy Parsons and [1*]Juliet A. Ellis

[1]The Randall Division of Cell and Molecular Biophysics, King's College, New Hunts House, Guy's Campus, London, SE1 1UL, U.K.

[2]Institute of Human Genetics, Fleischmannstr. 42/44, D-17487 Greifswald, Germany

[#] joint first author

* Corresponding author: Tel: +44 (0)20 7848 6498; Fax: +44 (0)20 7848 6435; e-mail: juliet.ellis@kcl.ac.uk

**Summary**

In-frame mutations in nuclear lamin A/C lead to a multitude of tissue-specific degenerative diseases known as the 'laminopathies'. Previous studies have demonstrated that lamin A/C-null mouse fibroblasts have defects in cell polarisation, suggesting a role for lamin A/C in nucleo-cytoskeletal-cell surface cross-talk. However, this has not been examined in patient fibroblasts expressing modified forms of lamin A/C. Here, we analysed skin fibroblasts from 3 patients with Emery-Dreifuss muscular dystrophy and from 1 with dilated cardiomyopathy. The emerin-lamin A/C interaction was impaired in each mutant cell line. Mutant cells exhibited enhanced cell proliferation, collagen-dependent adhesion, larger numbers of filopodia and smaller cell spread size, compared with control cells. Furthermore, cell migration, speed and polarization were elevated. Mutant cells also showed an enhanced ability to contract collagen gels at early time points, compared with control cells. Phosphotyrosine measurements during cell spreading indicated an initial temporal lag in ERK1/2 activation in our mutant cells, followed by hyper-activation of ERK1/2 at 2 hours post cell attachment. Deregulated ERK1/2 activation is linked with cardiomyopathy, cell spreading and proliferation defects. We conclude that a functional emerin-lamin A/C complex is required for cell spreading and proliferation, possibly acting through ERK1/2 signalling.

Key words: lamin A/C, laminopathies, ERK1/2 signalling, cell adhesion, cell spreading, Emery-Dreifuss muscular dystrophy.

## 1. Introduction

The LMNA gene is alternatively spliced to produce the two intermediate filament proteins termed nuclear lamin A and C (lamin A/C), which locate to the nuclear lamina, a fibrous structure underlying the inner nuclear membrane (reviewed in [1]). Lamin A/C interacts with many other nuclear proteins, including emerin (encoded for by the EMD gene), SUN- and nesprin-family members (reviewed in [2]). Mutations in either the LMNA or EMD genes result in the neuromuscular disorder Emery-Dreifuss muscular dystrophy, which is X-linked for EMD (X-EDMD; [3]) and autosomal (mainly dominant) for the LMNA gene (A-EDMD; [4]). Intriguingly, the LMNA gene is associated with an ever increasing number (currently tallying 16) of other tissue-specific degenerative diseases, which are collectively termed the 'laminopathies' (reviewed in [5]). These can be split broadly into two groups: i) neuromuscular disorders affecting directly the skeletal muscle, cardiac muscle and peripheral nervous system (e.g. A-EDMD, Limb-Girdle muscular dystrophy (LGMD1B), dilated cardiomyopathy (DCM); ii) partial lipodystrophy syndromes (FPLD) with or without developmental abnormalities and premature ageing such as Hutchison-Gilford Progeria Syndrome (HGPS). The laminopathies display extensive clinical variability, with both intra- and inter-familial variability observed within any one condition, suggesting that the genetic background plays a large role on clinical penetrance [6]. Moreover, although these diseases are clinically penetrant in patients in the heterozygous form, mouse models need to be homozygous to mimic the clinical phenotype [7-9].

Lamin A/C, emerin, and the LINC complex proteins SUN- and nesprin-family members, form a variety of macro-protein complexes at the nuclear envelope and together cross-link the nucleoskeleton to the cytoskeleton. These protein complexes function to maintain both nuclear architecture and cellular tensegrity [10-12]. Recently, it has been shown that the LINC complex is also 'hard-wired' to the cell surface. This involves the proteins giant nesprin-2 and nesprin-

3α at the outer nuclear membrane, interacting with micro- and intermediate filaments respectively, followed by a direct link to the cell adhesion receptors, integrins, via talin and plectin respectively [11, 13, 14]. This tight mechanical coupling created by the LINC complex allows for a direct physical signalling pathway from cell surface-mediated events to the nucleus and vice versa. Mutations in emerin, lamin A/C or nesprin-1/2 result in nuclear morphology defects, by proteins being either lost or mislocalised and to a disruption in chromatin-protein interactions, that leads to downstream gene expression tissue-specific effects [11, 15] For example, in skeletal muscle from EDMD patients interactions between the nuclear envelope and retinoblastoma (Rb) and MyoD proteins are disrupted at the point of exit from the cell cycle, delaying the onset of expression of genes involved in myogenic differentiation [16, 17]. However, in heart muscle, differentiation is suppressed by inappropriate activation of the extracellular-regulated kinase (ERK1/2) branch of the mitogen-activated protein kinase pathway and downstream targets (MAPK) [18, 19], implicated previously in both cardiomyopathy and cardiac conduction defects [20, 21].

Cell adhesion and polarisation defects are also linked to the absence of lamin A/C. $lmna^{-/-}$ MEFs (mouse embryonic fibroblasts) exhibit diminished ability to polarise at the edge of a wound [22-24], whereas this was normal in MEFs from both $Emd^{-/y}$ mice and in a mouse model for HGPS (which in this instance expresses no lamin A/C at the nuclear lamina [23]). Similarly, the activation of the small GTPase RhoA, a key regulator of cytoskeletal dynamics, and cell-substratum adhesion were decreased in both $lmna^{-/-}$ and HGPS MEFs, but not in $Emd^{-/y}$ MEFs [23]. These differences were attributed to both the degree of LINC complex disruption and the absence of lamin A/C from the nuclear envelope, with the $Emd^{-/y}$ mouse being least affected, since lamin A/C was correctly targeted to the nuclear lamina. However, no studies have been reported on possible cell surface effects in cells taken from laminopathy patients, and/ or in cells that express mutant forms of lamin A/C at the nuclear lamina. This is an important point to address since there is evidence suggesting lamin A/C-null mice models do not precisely

mimic the clinical situation e.g. desmin mislocalisation is not observed in EDMD patient myoblasts [25], but is in cardiomyocytes from lmna$^{-/-}$ mice [26].

Here, we set out to investigate whether nucleo-cytoskeletal-cell surface links are also perturbed in dermal fibroblasts taken from laminopathy patients expressing missense lamin A/C mutations associated with striated muscle diseases. We identified a reduction in the emerin-lamin A/C affinity alongside aberrant cell proliferation, adhesion and spreading and temporal changes in ERK1/2 activation. The severity of the molecular phenotype was mutation dependent. Together, this data highlights cell surface defects can occur in fibroblasts expressing modified forms of lamin A/C, as well as in cells null for lamin A/C. Furthermore, these defects arise directly from an impaired emerin-lamin A/C interaction, which may in turn affect LINC complex function.

## 2. Materials and Methods

### 2.1 Patients and cells

All individuals gave their informed consent for cell studies, which were approved by an institutional Ethics Review Board in Greifswald, Germany (Protocol number BB 35/07, approve date, August 03, 2007). Human dermal fibroblasts from three A-EDMD patients with the following lamin A/C mutations: R249Q (patient G-9666 in [27]), R453W (patient Spo89 in [28]) and patient G-8626 in [27]), the compound heterozygote R401C;T150HfsX5 (patient G-10877; [27], case 2 in [29]) and one DCM patient: R377H (patient G-12625, which we describe here for the first time), were cultured as primary cell lines. Clinical details of all of these patients except G-12625 are described in [27, 29]. Patients were aged 25, 34, 16 and 37 respectively at time of biopsy. Patient G-8626 died a few weeks after the cell cultures were established of sudden cardiac death (SCD). Patient G-10877 had inherited the R401C mutation from his mother, which was an amino acid change, classed as a genetic variant of unknown significance since she was clinically non-affected and the T150HfsX5 mutation (fsX5 means a

c.447insC generating a stop codon at c.459X predicted to produce a truncated protein) from his father, who suffered SCD, without prior skeletal involvement. Patient G-12625 presented at age 26 with an episode of tachycardia. When last examined at age 33, the patient presented with DCM and cardiac conduction defects without skeletal muscle involvement. Four other family members with the same clinical phenotype died from SCD in the 4$^{th}$ or 5$^{th}$ decade. However, other family members presented at a few decades after the onset of skeletal weakness, but before the cardiac complications, whereas other members developed no skeletal muscle disease at all. Interestingly, the R377H mutation is a recurrent mutation in the population and is associated with a range of other laminopathies such as LGMD1B with cardiac involvement [30] and adult onset proximal spinal muscular atrophy with cardiac involvement [31]. This mutation also exhibits variable penetrance and asymptomatic carriers have been reported [30, 32, 33].

Control dermal fibroblast cell lines were taken from two females (WT6000; aged 38 and WT6088; aged 55) and one male (WT6076; aged 35) without any known disease. All cell lines were grown in α-MEM (Gibco) supplemented with 10% FBS (Gibco) and 10 U/ml penicillin and 50 mg/ml streptomycin. Experiments were performed on cells between passage numbers 18 and 28.

**2.2 Lamin A/C protein expression levels and interaction with emerin.**

To determine total lamin A and C protein expression levels in our cell lines, lysates were prepared from cell samples of equal protein concentrations, and immunoblotted for lamin A/C (N-18; 1:1000 or Jol 5; 1:500), emerin (AP8; 1:2000) and as a loading control γ-tubulin (Sigma; 1:5000). Cell samples of equal protein concentration were co-immunoprecipitated in lysis buffer [34] for emerin-lamin A/C protein complexes as described in [35]. Samples were immunoprecipitated with anti-lamin A/C antibody N18 (1:100) and immunoblotted with anti-emerin antibody AP8 (1:2000). Interactions were quantified using densitometry (Gene Tools

analysis software, version 3.00.22, Synoptics Ltd) and expressed as a percentage of binding against total amount of emerin extracted.

**2.3 Cell proliferation assays.**

Sterile glass cover slips were coated with collagen (calf skin type I; used at 0.1% (w/v); Sigma) in 24-well plates and air-dried for 2 hours. Cells were plated at 5000/well in α-MEM + 10% FBS and fixed at 1, 3, 6 and 10 days after plating. Cell proliferation was assessed and changes in cell number quantified using the MTT [3-(4, 5-dimethylthiazol-2-yl)-2,5-diphenyltetrazolium bromide; Sigma No.M5655] metabolic viability colorimetric assay according to the protocol supplied by Sigma. To take into account cell size variation between cell lines, standard curves for dye uptake were performed on each cell line. Similarly, since the rate of cell adhesion (see below) also differed between the cell lines, we expressed changes in proliferation as a fold increase of the OD 570 nm value obtained on day 1 for each cell line. Cell proliferation was compared between the different cell lines over a range of comparable passage numbers (18-28). Each proliferation assay was repeated on three separate occasions, each time with triplicate samples. A senescence associated β-galactosidase staining assay was used to determine the senescence rate of our cell lines [36].

**2.4 Analysis of BrdU incorporation.**

To determine the proportion of cells in G0 of the cell cycle, sub-confluent cell cultures grown on collagen-covered cover slips in complete α–MEM + 10% FBS supplemented with 100 μM 5-bromo-2'-deoxyuridine (BrdU) for 72 hours. Cells were then fixed in 4% (w/v) paraformaldehyde (PFA) for 15 mins with 2M HCl treatment and permeabilised in 0.2% (v/v) Triton X-100 before staining with anti-BrdU antibody (1:100, Sigma) and counterstained with propidium iodide (5 μg/ml) to observe total DNA content. The percentage of BrdU (+) cells was determined for ~ 500 cells in multiple fields in 4 independent experiments. Those cells negative

for BrdU staining were considered to be in G0 phase of the cell cycle. Similarly, to determine the number of cells in S-phase, we first calculated the time point the cells entered S-phase. Cells were plated for 24 h, serum starved in α–MEM containing antibiotics for 72 h to synchronise cells into G0 (when only 1% of cells incorporate BrdU), re-stimulated with 10% FBS and pulse-labelled with 100 μM BrdU for 2 h at various times after re-stimulation to determine the entry point into S-phase. Cell samples were then fixed, stained with anti-BrdU antibodies and analysed as above.

**2.5 Immunofluorescent microscopy.**

Cells were fixed in methanol at -20°C and stained with anti-emerin (AP8, 1:100; [37] or anti-lamin A/C (N-18, 1:100; Santa Cruz), or fixed in 4% PFA/0.2% (v/v) Triton X-100 for 15 min before staining with anti-VASP (vasodilator-stimulated phosphoprotein, 1:100; Cell Signalling technology) or fixed in 4% (v/v) PFA for 15 min followed by permeabilisation in 0.2% (v/v) Triton X-100 before staining for integrin β1, α1, α2, (clone 4β7, 1:100; MAB1973, 1:250 and MAB1950, 1:250; Chemicon, respectively), anti-phosphotyrosine (clone 4G10, 1:500; Upstate Cell Signalling Solutions), talin (1:250, Sigma) or paxillin (1:250, BD BioSciences). F-actin was labelled with TRITC-phalloidin (1:500; Sigma). Secondary antibodies used were Chemicon fluorescent conjugates. Cover slips were mounted in Vectorshield containing DAPI (Vectorlabs). Fluorescent images were obtained using an Axiovert 200 M Zeiss inverted immunofluorescent microscope fitted AxioCam HR camera using a Plan Neofluar 40/0.57 Ph.2, ± Optiva x 1.6 and analysed using AxioVision Rel.4.6 (Carl Zeiss Inc) software. Confocal images were acquired on a Zeiss LSM 510 Meta confocal laser-scanning microscope using either x 25 or x 63 Plan-Neofluar oil immersion objectives.

**2.6 Rate of cell adhesion and collagen gel contraction assay.**

Cells were harvested, resuspended in α–MEM + 10% FBS and plated on either collagen I-or laminin-1 (Sigma, L2020) covered glass cover slips at 1 x $10^3$/well and immediately placed in an incubator at 37 ºC. At 10, 15, 30, 45, 60, 120 min after plating, non-adherent cells were gently washed off with PBS. The remaining cells were fixed and stained with TRITC-phalloidin as described above to ease cell visualisation. The total number of cells adhered to each cover slip was counted under x 10 phase objective, each sample was performed in triplicate, and the experiment repeated three times. For collagen gel contraction assays the method was used as described in [38]. Briefly, 10,000 cells were mixed with collagen I (final concentration 1 mg/ml) in a total volume of 100 µl and added to each well of a 96 well flat-bottomed plate and allowed to set for 90 min at 37 ºC. 100 µl of α-MEM + 10% FBS was added per well, the collagen plug carefully dislodged form the well sides with a needle and the plate returned to 37 ºC incubator. Phase-contrast images (x 0.11) of the collagen gels in their wells were collected over 24 h. 6 wells/ cell line were used and the experiment repeated five times. The degree of collagen contraction was measured using the image analysis programme, Image J, (http://rsb.info.nih.gov/ij/). In similar experiments, collagen gels were fixed in 0.1% glutaraldehyde at 2 and 24 h after the initiation of gel contraction and immunostained for F-actin. Z-stacks at 0.2 µm intervals were collected through the cells and a 3D reconstruction as a projected image and as an AVI were collected on a Leica confocal SP5 to examine cell morphological behaviour.

**2.7 Cell spreading and shape analysis.**

Cells were harvested, resuspended in α–MEM + 10% FBS and plated at 5 x $10^4$ cells/well of a 24-well plate containing collagen I-coated glass cover slips and incubated in a 37 ºC incubator. 3 cover slips were collected at time points between 10 min and 1 h and at 24 h after plating, and three independent experiments were performed. At collection, cover slips were gently washed in PBS, fixed and stained for focal adhesion proteins as described above. Cell samples were also

collected and immunoblotted for anti-total ERK1/2 (1:1000; Upstate Cell Signalling Solutions) and anti-phospho-ERK1/2 (1:1000; Cell Signalling technology). To calculate changes in cell shape during cell spreading images of cells stained with anti-VASP were collected using identical exposure settings in AxioVision Rel.4.6. For each cover slip, 5 fields where chosen at random and the area of 5 cells in each field was calculated (total of 25 cells/cover slip). Images were converted to 8 bit greyscale Tiff files and imported into Mathematica 6.0 (Wolfram Research, Champaign, IL, USA) where they were auto-levelled, de-noised using a 5 x 5 low-pass filter, auto-levelled again and thresholded to give black and white images in which white pixels represented the footprint of the cell, whilst the black pixels represented background. Further analysis in Mathematica 6.0 yielded the following 2 cell shape parameters based on statistical moments analysis: cell area (in $\mu m^2$) and elongation (ratio of the longest axis to the shortest axis expressed as a value of $2^n$, where n is the power you need to raise to give that ratio) [39]. From the same anti-VASP stained images, we also counted the number of filopodia/cell, where we defined a protrusion as projecting a minimum of 2 μm out from the actin cortical ring, measured using the Image J programme. Similarly, we calculated the percentage of the cell area occupied by focal contacts (FCs) at each time point by converting our anti-VASP stained images to 8-bit TIFF files and imported into Mathematica 6.0. These were auto-levelled followed by de-noising using a 5 x 5 low-pass filter. Next, images were subjected to a 25 x 25 high-pass filter to accentuate regions containing pixels that had large differences in intensity followed by further auto-levelling. The combination of the two filters affects a band-pass filter that enhances the intensity of FCs, whilst suppressing objects that are smaller or larger than these. The band-pass filtered image was then thresholded to give a binary image consisting of white FCs on a black background. The Mathematica 6.0 program from which this was derived can be seen in [40].

**2.8 In vitro scratch and cell motility assays.**

Cells in α-MEM + 10% FBS were plated at 1.5 x $10^5$/well of a collagen-coated 12 well plate, to achieve confluent monolayers within 24 hours of plating. A scratch was scored across the centre of each monolayer with a plastic pipette tip. Pre-warmed α–MEM/25mM HEPES was added, the plate sealed and placed in a pre-heated chamber (37 ºC) on an inverted Axiovert 200 Zeiss microscope fitted with an Sensicam CCD camera (P.C. Cooke). Cells were allowed to equilibrate and phase contrast images were collected across the wound under x 5 objective at 1 picture per 10 min over 20 h. Similarly, to examine single-cell motility behaviour, cells were plated at 2 x $10^4$/ well, allowed to adhere for 15 min and images collected with x 5 phase objective every 3 min for 2 h. In the scratch assay at least 30 cells and in the cell motility assay at least 50 cells, from 3 and 6 wells respectively were analysed for changes in mean speed and mean persistence. Time-lapse image series in TIFF format were imported into Mathematica 6.0 and the xy-co-ordinates of individual cells determined at different time points using our own Mathematica 6.0 cell tracking program. The persistence and speed of cell movement was then determined from these co-ordinates. Persistence was calculated by dividing the distance between the first and last point, i.e., distance as the crow flies, by the actual distance covered by the cell (by summing inter-frame distances across the whole time series). Values tending towards one indicate cells moving in a straight line, whereas values tending towards zero indicate random motion. Speed was determined by dividing the inter-frame distances by the amount of time between frames captured and is expressed in μm/hour. The values presented represent the mean speed across all frames per time-series.

**2.9 Statistical analysis.**

All measurements are given as mean ± SEM. The statistical significance was assessed using the two sample assuming equal variance student t-test, except for quantifying the immunoprecipitation and pERK experiments where it was determined by performing an ANOVA test followed by Dunnett's multiple comparison test.

## 3. Results

### 3.1 Lamin A/C expression and nuclear localisation.

The dermal fibroblasts expressing the R453W, R249Q or R401C;T150HfsX5 (hereafter referred to as R401C) mutations used in this study have been characterised previously between passages 1 and 11 for lamin A/C protein expression levels, nuclear antigen localisation and structure (Fig. 1A) [27]. Briefly, they showed that fibroblasts expressing only the R401C and R453W mutations exhibited extreme nuclear abnormalities with lamin A/C displaying a honeycomb or intra-nuclei foci localisation, respectively. No nuclear abnormalities were reported for the R249Q cell line. Although they also analysed a cell line expressing the R377H mutation, this was from a different patient to the one reported in the study here. Since we received the cell lines at higher passage numbers (between 5 and 18) we re-evaluated these parameters and characterised the cell line expressing the R377H mutation. Our findings for the nuclear localisation of lamin A/C and emerin (data not shown) were consistent with that reported by [27]. Our cell line expressing the R377H mutation exhibited normal nuclear architecture, in agreement with the cell line expressing the same mutation reported in [27]. We also immunoblotted the cell lines for emerin and lamin A/C using used two anti-lamin A/C antibodies; N18 (epitope in first 50 residues) and Jol 5 (epitope within the first 117 residues) to counter the possibility of epitope masking arising from the lamin A/C mutations skewing the antibody recognition. Both antibodies gave the same immunoblotting results and those for N18 at passage 22 are shown (Fig. 1B). We found that lamin A/C levels remained stable as passage number increased, in both the normal controls and mutants, but levels were consistently slightly less in the R337H and R249Q mutant cell lines. Additionally, emerin was slightly reduced in the R249Q cells. Unexpectedly, the R401C mutant cell line expressed near normal levels of lamin A/C, as reported previously [27] despite the prediction that the T150HfsX5 mutation severely

truncates the lamin A/C protein so that it is unlikely to be translated. This suggests that protein expression from the allele carrying the R401C mutation is upregulated.

### 3.2 Emerin-lamin A/C interaction is impaired.

Emerin's binding site in lamin A/C spans residues 384-566, which includes the R453W and R401C mutations [41], but there are data to suggest that residues outside of this region additionally influence emerin binding through uncharacterised secondary mechanisms [35, 42, 43]. To date, only one study has examined whether the emerin-lamin A/C is impaired by LMNA mutations in vivo (R401C-alone and R482L; [43]) and thus it is not known if the emerin-lamin A/C interaction, is consistently affected by LMNA mutations. We immunoprecipitated our cell lines with anti-lamin A/C N18 antibody and immunoblotted for emerin. Significantly less emerin was pulled down with the mutant lamin A/C proteins than with our normal controls, with the R401C being the most affected (17% less; Fig. 1C and D). We have previously shown that the LMNA T150P mutation abolished all interaction with emerin in vitro [35], whereas the R401C-alone mutation has been reported to interact normally with emerin in vivo [43]. It appears that mutations at residue R401 somehow reduce the severe effect mutations at residue T150 cause. Interestingly, all of the LMNA mutations used in this study are predicted to not affect lamin dimer formation, but to perturb higher filament formation needed for nuclear lamina structure and function [44]. Coupled with the lower binding affinity between emerin and lamin A/C, we propose that the nuclear lamina-nuclear envelope link is functionally compromised in the patient fibroblasts used in this study.

### 3.3 LMNA mutations leading to EDMD/DCM increases cell proliferation.

Cell hyper-proliferation is observed in the absence of lamin A/C in $lmna^{-/-}$ MEFs [45, 46] and with the missense EDMD mutation R453W expressed in a stable myoblast cell line [47]. However, in patient dermal fibroblasts homozygous for the LGMD1B-causing mutation Y259X,

which results in cells expressing no lamin A/C, there is a decrease in cell growth [48, 49]. Clinically, the vast majority of the laminopathies arise from in-frame LMNA mutations affecting one allele, and thus a modified form of lamin A/C is expressed alongside normal lamin A/C. To date, cell proliferation has not been examined in cells expressing this genotype, and we set out to investigate this. We calculated cell proliferation curves for three controls and three EDMD- and one DCM-derived dermal fibroblast cell lines at comparable passage numbers (18-22). Phase contrast micrographs illustrate that all of the mutant cell lines proliferated faster than all three controls (Fig. 2A). Proliferation was quantified using the MTT assay as the fold increase over day 1 for each cell line (Fig. 2B). The R401C cell line displayed the greatest increase in proliferation followed by R453W and R249Q, with R377H being only slightly elevated over the average for the 3 controls. Senescence (1.5-2% of all cells) was unchanged at comparative passage numbers across all control and mutant cell lines over this time course according to the senescence-associated β-galactosidase activity assay (data not shown). Thus, changes in senescence rates were not contributing to the differences in cell proliferation.

We then examined whether the alterations in cell growth could be attributed to a defect in cell cycle progression. We first calculated the point of entry into S-phase from G0 which was 16 h for the control cell lines and between 11 (R401) and 15 (R377H) h for mutant cell lines (data not shown). BrdU positive cells were then counted at 2 hours after entry into S-phase. Consistent with the earlier S-phase entry time for the mutant cell lines, a larger proportion of proliferating mutant cells were in S-phase, compared with the three controls (Fig. 2C). Once again the R401C mutant was the most affected, with 53% of cells in S-phase, followed by R453W and R249Q, with R377H the least at 33%, compared to an average for the 3 controls of 28% (Fig. 2C). These findings could not be fully attributed to a decrease in the number of quiescent cells, since there was only a slight decrease in the proportion of mutant cells in G0 compared to an average of the 3 controls (Fig. 2C). Together these results suggest a change in

the timing of entering S-phase contributes to changes in cell proliferation, with the value of the change dependent on the specific LMNA mutation.

**3.4 Cell adhesion onto collagen is elevated by LMNA mutations.**

Cell proliferation is also dependent on growth regulatory effects associated with cell adhesion and cell size. There are no prior reports of EDMD/DCM cell lines being investigated in this manner. To initiate such a study, we first examined the rate of cell attachment onto either collagen- or laminin-1-coated cover slips. Both the mutant and control cell lines adhered to laminin-1 at the same rate (data not shown), where as all the mutant cell lines displayed an enhanced initial rate of cell attachment over the three control cell lines onto collagen (Fig. 3). This trend continued until about 45 minutes after plating, but by 1 hour was noticeably less marked. By 2 h the total number of attached cells was similar for both mutant and control cell lines. The R401C cell line attached the fastest (x 2.05 over controls), followed by R453W and R249Q, with R377H the slowest (x 1.41 over controls), but was statistically significant over the controls. This direct correlation between a particular LMNA mutation and the changes to both cell adhesion and proliferation, suggest the LMNA mutations are functionally responsible for these observed molecular phenotypes. Changes in cell-substratum adhesion have also been reported in $lmna^{-/-}$ MEFs, but here it was decreased [23]. Collectively these data reinforce the theory that a functional nuclear lamina is required for normal cell adhesion and this can be perturbed in a LMNA mutation-specific manner.

**3.5 LMNA mutations reduce cell spreading on collagen substrate.**

Cell adhesion rate is dependent on the rate of formation of focal contacts (FCs). Cells modulate adhesion by controlling the surface density, state of aggregation and activation of adhesion receptors. We next examined the formation of FCs over 24 h, by imaging spreading cells for a range of integrin subunits and components of FCs, F-actin, emerin and lamin A/C. We observed

no morphological alterations to the nuclei or any re-distribution of emerin or lamin A/C during cell adhesion and spreading in either mutant or control cell lines (data not shown). Similarly, the distribution of the collagen receptor integrin subunits α1, α2 and β1, the laminin-1 receptors integrin subunits α6 and α7 or the FC proteins talin and paxillin were not perturbed in the mutant cell lines during cell adhesion (data not shown).

Following cell attachment, and in the absence of a chemotactic stimulus, cells spread to achieve the cell mass required for cell division. We next analysed the cell spreading phenomenon by staining both control and mutant cells for VASP, which binds to and thus labels the barbed ends of F-actin, FC components, lamellipodia and filopodia tips. Anti-VASP stained cell images were band-pass filtered, thresholded to extract fluorescent structures corresponding to FCs and shown as a binary image alongside the corresponding anti-VASP stained image (labelled as FC in Fig. 4A). Aberrant cell spreading features were observed to affect 50-60% of the cell population for each mutant cell line. We show cell images from the R401C and WT6000 cell lines in Fig. 4A and use the data collected to form Fig. 4A to calculate the data presented in Fig. 4B-D. We first calculated the percentage of the total cell area covered by FCs. This demonstrated that at each time point, approximately x 1.5 fold increase in cell area was occupied by FCs in the mutant cells than in the controls (Fig. 4B). This FC 'crowding' distorted observations of possible visual changes in individual FC arrangement, morphology or numbers.

Next, we quantified the number of filopodia, cell area and cell elongation changes during cell spreading. Two striking differences were observed as early as 10 min after plating. Firstly, mutant cells produced greater numbers of filopodia and few or no ruffles compared to controls at each time point, a feature that persisted until 1 hour when filopodia levels normalised to that of the control cells (Fig. 4C). Secondly, although cell area increased steadily with spreading time for both control and R401C cells, at each time point the total cell area was considerable less for the mutants than the control cells and by 1 hour was still only 55% of control levels (Fig. 4Di). The reduction in cell area of the R401C mutant was consistent with its slightly lower

elongation values compared to controls (Fig.4 Dii). The other mutant cell lines also exhibited these changes in cell spreading behaviour, but were not as severe as the R01C cell line. It is noteworthy that by 24 hours after plating, all of these parameters were similar between the mutant and control cell lines, suggesting that it is only early events in cell adhesion/spreading that are disrupted. This may explain why cell spreading defects have not been previously associated with LMNA mutations, since studies have concentrated on cells plated for at least 24 h. Together, these results suggest that cell adhesion and spreading are influenced by nuclear antigen functionality, affirming the theory that nucleo-cytoskeletal links can be extended to include the cell adhesion machinery at the plasma membrane.

**3.6 Disorganised F-actin network and impaired phosphorylation of FC components.**

We also stained spreading cells for F-actin and under confocal microscopy this revealed that the F-actin network was slightly more disorganised in the mutant cells compared with control cells, notably with earlier production of cortical actin and stress fibre retention at 24 h. We show cell images representing this finding from the R401C and WT6000 cell lines in Fig. 5. Confocal microscopy confirmed our earlier findings of the mutant cells producing more filopodia. Previous studies on $lmna^{-/-}$ MEFs also revealed minor disorganisation of the microfilament, microtubule and intermediate filament networks, most marked in the regions close to the perinuclear region [12]. It is interesting to note that F-actin is also a binding partner of lamin A/C, which binds through lamin A/C's C-terminal domain (residues 563-646) [50]. Impairment of this interaction arising from secondary effects of the LMNA mutations may contribute to the F-actin network disorganisation and in turn compromise emerin-lamin A/C complex function.

Integrin clustering rapidly induces tyrosine phosphorylation of intracellular FC adapter proteins, promoting intermolecular SH-2-phosphotyrosine interactions required for FC assembly [51]. Analysing the phosphotyrosine level on FC components gives an indication of their

activation status. To examine for this, we immunostained our spreading cells with an anti-phosphotyrosine antibody. Phosphotyrosine-positive FC staining was less pronounced in the mutant cells than in the control cells at 15 minutes post-attachment (Fig. 5A). Since it is already known that deregulated MAPK-ERK1/2 signalling precedes the development of the cardiomyopathy in EDMD [18, 19] and that ERK1/2 signalling contributes to the regulation of cell spreading [52], we next examined ERK1/2's phosphorylation (pERK1/2) level during cell spreading. Analysis with anti-phospho-p44/42 MAPK-ERK1/2 (T202/Y204) and anti-total MAPK-ERK1/2 antibodies respectively identified a significantly reduced pERK1/2 at both 15 and 30 min after plating in our mutant cell lines. At 2 h post-attachment, when cell spreading is completed, pERK1/2 was elevated in both control and mutant cell lines, but was significantly higher in the mutant compared to the control. Active pERK1/2 is associated with cell proliferation and elevated pERK1/2 in laminopathy affected cells or tissues has been reported previously [18, 19, 53]. We hypothesise that a temporal delay in ERK1/2 activation is likely to be a major contributing factor to the early reduction in cell area during cell spreading in fibroblasts expressing LMNA mutations.

**3.7 Increased collagen gel contractility.**

Three-dimensional collagen gels allow for an in vivo approach to study the ability of the cytoskeleton to provide the necessary tensional force to counteract the mechanical load generated by the extracellular matrix. Fibroblast cell lines were resuspended in a collagen gel matrix then the set gel released from the sides of the plate, so as to remove the tensional forces generated by the collagen. We calculated the percentage of gel contraction over time and found that the collagen gel contracted faster when it contained mutant cells compared to control cells. A representative experiment showing the gel contraction in a 96-well plate for the R401C and WT6000 cell lines is shown in Fig. 6A. Quantification of gel areas demonstrated that the mutants exhibited an accelerated rate of gel contraction at the early time points up to 4 h, and

then begun to tail off. By 10 h the gels containing the mutant and control cells contracted at a similar rate (Fig. 6B). We analysed the F-actin network of the cells in the collagen gels using confocal microscopy. Overt changes in the basal actin cytoskeleton were observed between the mutant and control cells. 2h after gel release, the control cells were still reasonably rounded in shape with few filopodia projections, whereas the majority of the mutant cells were larger and had protrusions of many fine filopodia. (Fig. 6B, 2h insets). The increase in early numbers of filopodia was consistent with our cell spreading experiments performed on a rigid substrate (Fig. 4A). By 24 h the control and mutant cells were indistinguishable in cell shape, both appearing elongated with similar numbers and shape of filopodia (Fig. 6B, 24 h insets). We conclude that the collagen gel hyper-contractility observed in the mutants arises from their ability to form more and earlier cell-substratum interactions in the early stages of cell spreading, than our control cells.

**3.8 Both polarized and random cell migration are elevated in the mutant cell lines.**

We next investigated whether the LMNA mutations resulted in cell migratory defects. Cells were imaged using phase contrast time-lapse microscopy and individual cells were tracked and analysed to determine migration speed. Data demonstrates that mutant cells migrated more rapidly than their normal control counterparts (Table 1, Supplementary data). We also used a scratch assay to determine if our mutant cells exhibited defective polarized motility. Again the mutant cells exhibited a significant increase in migration speed over the normal controls. In both experiments the cell lines exhibited similar mean persistence, indicating that the mutant cells underwent corresponding polarised cell migratory trajectories to normal controls (Table 1, Supplementary data). This is the first report examining the effect of LMNA mutations on random cell migration. Previous reports examined only polarized cell migration in scratch assays. MEFs from $lmna^{-/-}$ mice exhibited diminished polarized cell migration, whereas MEFs from $Emd^{-/y}$ and HGPS mice were unaffected, [22, 23]. Once again, these data reinforce the

theory that a functional nuclear lamina is required for cell surface mediated events, in this case cell migration, and that this can be perturbed in a LMNA mutation-specific manner.

## 4. Discussion

### 4.1 Missense LMNA mutations affect cell cycle progression.

It is well established that mutations in either the LMNA or EMD genes alter cell cycle kinetics [37, 45-47, 54, 55]. For the LMNA gene, most studies have been performed on the null phenotype and so it is unclear if there are any mutation-specific effects. Here, we demonstrate a significant increase in cell proliferation associated with EDMD-, but not DCM-causing mutations. Similarly, normal cell cycle timing is associated with fibroblasts from FPLD patients [43, 47], whereas a decrease in cell growth rate occurs in fibroblasts from HGPS patients [54]. Although only one each of a DCM, HGPS and FPLD-derived cell lines have been analysed for cell proliferation defects, collectively these findings infer laminopathy-specific effects. The increase in cell numbers of mutant cells versus control cells entering S-phase in our EDMD/DCM cell lines lie between those reported for the $lmna^{-/-}$ MEFs and retinoblastoma-null MEFs [45], whereas S-phase block developed with increasing passage number in HGPS patient cells [54]. Johnson et al attributed the S-phase anomalies to a commensurate decrease in the percentage of cells in both G1- and G2/M-phases and by inference, a similar mechanism may also be occurring in the EDMD cell lines studied here.

Two mechanisms have been proposed to explain the increase in cell proliferation associated with LMNA mutations. Firstly, defective TGF-β1-Rb-SMAD signalling in $lmna^{-/-}$ MEFs was found to increase their proliferation potential [46] and secondly, a failure of nuclear envelope-Rb/MyoD interactions at the point of exit from the cell cycle has been found to delay myogenic differentiation [16, 17]. However, other signalling pathways that control cell proliferation may also be involved. For instance, the MAPK-ERK1/2 signalling cascade regulates cell proliferation as well as survival, growth and differentiation [56, 57]. Active

ERK1/2 (which is phosphorylated; pERK1/2) is expressed during cell proliferation and must be de-activated for cell differentiation to occur. Both our patient and control cells exhibited an increase in pERK1/2 activity after the completion of cell spreading, as expected for cells entering the cell cycle. However, pERK1/2 was hyper-activated in the mutant cell lines compared with the control cells. This is consistent with the finding that hyper-activated pERK1/2 has been found in cardiac tissue from lmna$^{-/-}$ mice and in HeLa fibroblasts and C2C12 myoblasts in which lamin A/C has been knock-down by siRNA [18, 19, 53]. Perturbed ERK1/2 signalling is therefore likely to contribute to the observed proliferation defect associated with LMNA mutations.

**4.2 Aberrant cell adhesion, spreading and migration induced by LMNA missense mutations.**

Integrin engagement stimulates the Ras-activated MAPK-ERK cascade associated with cell growth and proliferation. Activated ERK1/2 translocates to newly formed FCs [58] where it associates with paxillin [59]. Cells deficient in MEK1, the upstream activator of ERK1/2, display increased cell adhesion and reduced cell spreading [52] directly implicating ERK1 signalling in cell spreading. Active ERK1/2 at FCs promotes the phosphorylation and thus activation of myosin-light chain kinase (MLCK), resulting in increased actomyosin contractility. This promotes FC disassembly an essential process to allow cell spreading to proceed [60].

The results we present here implicate delayed ERK1/2 signalling is contributing to the slower cell spreading phenotype observed in our laminopathy patient cells. Others have shown that suppression of ERK1/2 activity prevents its movement to the FCs [58], which in turn would impede MLCK activation, ultimately reducing cell spreading. However, we observed an increase in the initial stages of contractility in the mutant cells during the initial stages of cell spreading in collagen gels, suggesting earlier activation of MLCK. Cells behave differently when spreading on rigid materials such as collagen coated cover slips, compared with spreading

in softer substrates such as collagen gels [61]. Therefore a direct comparison of cell spreading phenotype between these substrata needs to be interpreted with caution. Nevertheless, it is possible that the enhanced activation of ERK1/2 we observed 2 hours post-attachment of cells spreading on collagen-covered cover slips, may occur earlier in collagen gels, which would explain the earlier MLCK activation. Notwithstanding this, many kinases regulate MLCK activity and future work is needed to elucidate the exact mechanism behind this.

A substrate-dependent effect was observed with respect to the increase in cell adhesion observed in the mutant cell lines. Since the integrin subunits involved in cell adhesion to both collagen or laminin-1 substrate localised normally throughout cell spreading, it is likely an inside-out signalling pathway is involved. We are currently investigating this finding.

We also show here that both random and polarized cell migration are elevated in our mutant cells compared to controls. This is the first time random cell migration has been shown to be affected by LMNA mutations. The increased cell motility may arise, at least in part, from the increased proliferative capacity of the mutant cells. But taking our findings on increased cell motility with both the increases in cell adhesion and FC coverage shown in Figs. 3 and 4, we can speculate that the mutant cells are likely to be forming increased numbers of smaller FCs. This would result in an initial increase in cell adhesion, but permit faster disassembly of the FCs, elevating cell motility.

### 4.3 Lamin A/C modulates pERK1/2 activation through a direct interaction

MAPK cascades are traditionally activated by either GPCR or RTK signalling pathways and so it is not immediately obvious as to how this could occur from a primary effect originating from a mutation in nuclear lamin A/C. A recent publication sheds some light on this dilemma. Lamin A/C is a binding partner of both pERK1/2 and the transcription regulator c-Fos [62]. Lamin A/C sequesters c-Fos to the insoluble nuclear fraction preventing it from activating AP1-mediated transcription. Activated ERK1/2 binds to lamin A/C, releasing c-Fos from lamin A/C,

so that c-Fos can now be activated by pERK1/2. Consistent with this mechanism, lmna$^{-/-}$ MEFs exhibit increased AP1-mediated transcription compared with control cells [62]. The nuclear lamina can thus act as a scaffold for components of the MAPK-ERK1/2 pathway [62]. Taking the Gonzalez et al results with the data we present in this paper, we would like to propose that either the presence of modified forms of lamin A/C or its total absence from the nuclear lamina perturbs the nuclear lamina structure sufficiently to directly affect both nuclear ERK signalling and delay ERK1/2 activation required for cell spreading.

In conclusion, our study has shown for the first time that cells from laminopathy patients' exhibit perturbed cell surface signalling as reported previously in the lamin A/C-null models. Our results also suggest a correlation can be made between the genetic lesion and how severely affected a particular molecular pathway is. The R401C;T150HfsX5 mutation consistently disrupted the phenotypes analysed in this paper significantly more than the 3 other mutations examined, particularly compared with the R377H mutation which clinically resulted in DCM-alone in this instance. Finally, it is interesting to note that mutations in either MEK1 or MEK2, give rise to cardio-facio-cutaneous syndrome [63]. This is a developmental delay disorder involving craniofacial, cardiac, hypotonia and ectodermal abnormalities. Uniquely to disorders associated with the Ras-pathway it is caused by missense mutations alone, as is the case for the laminopathies. Exogenous expression of these mutations produces hyperactivation of pERK1/2. Together these findings highlight the importance of MAPK-ERK1/2 signalling in both cell fate and subsequent tissue development.

## 5. Figure Legends

**Fig. 1.** Characterisation of cell lines used in this study. (A) Domain structure of human lamin A indicating disease-causing mutations used in this study. Lamin A consists of a central rod region of α-helical segments (coil 1a, 1b, 2a and 2b) and N- and C-terminal globular tails. Numbers refer to amino acid residues in the primary sequence. Lamin C is similar in structure, but is

alternatively spliced at residue 566 with a unique 6 residue tail added. The positions of the mutations used in this study are marked by double-headed arrows. Figure adapted from [35]. The emerin binding site is marked with a bold under-line. (B) Immunoblot of the expression levels of lamin A/C and emerin in wild type and mutant dermal fibroblasts. 10 μg of cell lysates from non-synchronised cultured fibroblast cell lines all at passage 22 (3 controls, WT6000, WT6076, WT6088, 3 A-EDMD patients and 1 DCM patient) were loaded on 10% SDS-PAGE gels and immunoblotted with anti-lamin A/C antibody N18, anti-emerin antibody AP8 and anti-γ-tubulin antibody as a protein loading control. (C) Co-immunoprecipitation of emerin with lamin A/C. Protein lysates of equal starting concentration were immunoprecipitated with anti-lamin A/C N18 antibody. Eluted bound (B) and unbound (S) protein samples were separated by 10% SDS-PAGE and immunoblotted for emerin. The experiment was repeated 3 times and we show a representative example with control cell line WT6000. The lane marked 'control' is the co-immunoprecipitation performed only with the pre-immune serum. (D) Binding from the 3 individual co-immunoprecipitation experiments was quantified by densitometry (Gene Tools analysis software version 3.00.22, Synoptics Ltd), averaged and shown as percentage bound of the total amount of emerin present. The lane labelled 'WTav' represents an average value for the 3 control cell lines, WT6000, WT6076 and WT6088. n = 3; * * = $p < 0.01$ for mutants compared with WTav.

**Fig. 2.** Mutant cells exhibit increased proliferation. (A) Phase contrast micrographs of each of our patient cell lines and 3 control cell lines (WT6000, WT6076, WT6088) grown on collagen-covered cover slips were taken 1, 3, 6 and 10 days after seeding at equal cell density. Bar; 100 μm. (B) Cell proliferation was determined at 1, 3, 6 and 10 days after plating by the MTT assay. Standard curves were performed for each cell line to control for cell size differences and variation in dye uptake between each cell line (data not shown). Results are shown as the fold increase in the OD 570 nm value for day 1 for each cell line. The data shown represent the

average for three independent experiments, with each performed in triplicate. 'WTav' represents average values for the 3 control cell lines, WT6000, WT6076 and WT6088. n = 3; $p < 0.05$ for all mutant cell lines compared with the value for WTav. (C) BrdU incorporation to determine the proportion of cells in GO and in S-phase. The data shown represent the average for three independent experiments each performed in triplicate. 'WTav' represents average values for the 3 control cell lines, WT6000, WT6076 and WT6088. n = 3; ** = $p<0.01$

**Fig. 3.** Cell adhesion on to collagen. Cells were plated at 1 x $10^3$cells/well on to collagen-coated cover slips in the present of serum and fixed at time intervals up to 2 hours after plating. The total number of cells adhered to each collagen coated cover slip were counted under x 10 phase objective. The data shown represent the average of three independent experiments. 'WTav' represents average values for the 3 control cell lines, WT6000, WT6076 and WT6088. n = 3; ** = $p < 0.01$, * = $p < 0.05$ for the mutant cell lines compared with the value for WTav.

**Fig. 4.** Cell spreading on collagen. Cells from the control cell line WT6000 and the patient expressing the R401C mutation are illustrated in this figure. (A) Cover slips were collected at times shown after cell plating in the presence of serum, fixed and stained with anti-VASP antibody. Anti-VASP stained cell images were band-pass filtered, thresholded to extract fluorescent structures corresponding to FC and shown as an auto-levelled binary image alongside the corresponding anti-VASP stained image (labelled as 'FC'). Bar, 20 μm. (B) Images collected for the analysis of FC distribution in (A) were analysed for FC coverage. The total numbers of pixels representing FC in the thresholded images were divided by the number of pixels representing the whole cell area. This is expressed as a percentage of cell area. n = 25; ** = $p < 0.01$, * = $p < 0.05$ for the R401C mutant cell line compared with the value for WT6000. (C) From the images captured in (A), we counted the number of filopodia (defined as a pointed appendage projecting at least 2 μm from the actin cortical ring) over the first hour of

spreading. n = 25; ** = $p < 0.01$ for the R401C mutant cell line compared with the value for WT6000. (D) From the images captured in (A) we calculated the cell area (i) and elongation (ii) over 24 hrs after cell plating. n = 25; * = $p < 0.05$ for the R401C mutant cell line compared with the value for WT6000.

**Fig. 5.** Tyrosine phosphorylation during cell spreading. Cells from the control cell line WT6000 and the patient expressing the R401C mutation are illustrated in this figure. (A) Cover slips were collected at 15 min, 30 min, 2 h and 24 h after cell plating, fixed and stained with the anti-phosphotyrosine antibody (green) and TRITC-phalloidin for F-actin (red). Bar; 20 μm. (B) Cell samples were collected at 15 min, 30 min and 2 h after plating and immunoblotted for total ERK1/2, pERK1/2 and α-tubulin as a protein loading control. We show a representative blot. (C) Immunoblot band intensities from the 3 independent experiments shown in (B) were quantified by densitometry (Gene Tools analysis software version 3.00.22, Synoptics Ltd), averaged and shown as ERK activity (pERK/total ERK). n = 3; * * = $p< 0.01$ for the R401C mutant cell line compared with the value for WT6000.

**Fig. 6.** Collagen gel contraction. (A) A collagen gel assay was performed in the presence of serum as described in Materials and Methods. Five separate experiments were performed, each with 5 samples. Phase contrast images (x 0.11) were collected over a 24 hour time course after plating. A representative example of the contraction gel 96-well plate is shown at 4 and 24 h for the control cell line, WT6000 and the patient expressing the R401C mutation. (B) From the collected images, the degree of collagen contraction was calculated from the change in area of the collagen gel as a function of time, using the image analysis programme, Image J. n = 5; ** = $p < 0.01$ for the R401C mutant cell line compared with the value for WT6000. Collagen plugs were fixed at time points 2 and 24 h and the F-actin distribution (green) and nuclei (blue) distribution in the individual cells were captured under confocal microscopy. Bar, 10 μm.

**Supplementary data**

**Fig. 1.**

The data used to formulate Table 1 are presented here for the (A) scratch assay and (B) cell motility assay. We show data from the control cell line, WT6000 and the patient expressing the R401C mutation. For the scratch assay at least 30 cells from 3 wells and for the cell motility assay at least 50 cells from 6 wells were analysed for mean persistence and mean speed as described in the Materials and Methods. For mean persistence, a value tending towards one indicates cells moving in a straight line, whereas values tending towards zero indicate random motion. Mean speed values are shown in μm/hour.

**6. References**


1. Gruenbaum, Y., Margalit, A., Goldman, R. D., Shumaker, D. K., and Wilson, K. L. (2005). The nuclear lamina comes of age. *Nat Rev Mol Cell Biol* **6,** 21-31.
2. Zastrow, M. S., Vlcek, S., and Wilson, K. L. (2004). Proteins that bind A-type lamins: integrating isolated clues. *J Cell Sci* **117,** 979-87.
3. Bione, S., Maestrini, E., Rivella, S., Mancini, M., Regis, S., Romeo, G., and Toniolo, D. (1994). Identification of a novel X-linked gene responsible for Emery-Dreifuss muscular dystrophy. *Nat Genet* **8,** 323-7.
4. Bonne, G., Di Barletta, M. R., Varnous, S., Becane, H. M., Hammouda, E. H., Merlini, L., Muntoni, F., Greenberg, C. R., Gary, F., Urtizberea, J. A., Duboc, D., Fardeau, M., Toniolo, D., and Schwartz, K. (1999). Mutations in the gene encoding lamin A/C cause autosomal dominant Emery-Dreifuss muscular dystrophy. *Nat Genet* **21,** 285-8.
5. Ellis, J. A. (2006). Emery-Dreifuss muscular dystrophy at the nuclear envelope: 10 years on. *Cell Mol Life Sci* **63,** 2702-9.
6. Bonne, G., Yaou, R. B., Beroud, C., Boriani, G., Brown, S., de Visser, M., Duboc, D., Ellis, J., Hausmanowa-Petrusewicz, I., Lattanzi, G., Merlini, L., Morris, G., Muntoni, F., Opolski, G., Pinto, Y. M., Sangiuolo, F., Toniolo, D., Trembath, R., van Berlo, J. H., van der Kooi, A. J., and Wehnert, M. (2003). 108th ENMC International Workshop, 3rd Workshop of the MYO-CLUSTER project: EUROMEN, 7th International Emery-Dreifuss Muscular Dystrophy (EDMD) Workshop, 13-15 September 2002, Naarden, The Netherlands. *Neuromuscul Disord* **13,** 508-15.
7. Sullivan, T., Escalante-Alcalde, D., Bhatt, H., Anver, M., Bhat, N., Nagashima, K., Stewart, C. L., and Burke, B. (1999). Loss of A-type lamin expression compromises nuclear envelope integrity leading to muscular dystrophy. *J Cell Biol* **147,** 913-20.
8. Mounkes, L. C., Kozlov, S. V., Rottman, J. N., and Stewart, C. L. (2005). Expression of an LMNA-N195K variant of A-type lamins results in cardiac conduction defects and death in mice. *Hum Mol Genet* **14,** 2167-80.
9. Arimura, T., Helbling-Leclerc, A., Massart, C., Varnous, S., Niel, F., Lacene, E., Fromes, Y., Toussaint, M., Mura, A. M., Keller, D. I., Amthor, H., Isnard, R., Malissen,

M., Schwartz, K., and Bonne, G. (2005). Mouse model carrying H222P-Lmna mutation develops muscular dystrophy and dilated cardiomyopathy similar to human striated muscle laminopathies. *Hum Mol Genet* **14,** 155-69.

10. Lammerding, J., Schulze, P. C., Takahashi, T., Kozlov, S., Sullivan, T., Kamm, R. D., Stewart, C. L., and Lee, R. T. (2004). Lamin A/C deficiency causes defective nuclear mechanics and mechanotransduction. *J Clin Invest* **113,** 370-8.
11. Crisp, M., Liu, Q., Roux, K., Rattner, J. B., Shanahan, C., Burke, B., Stahl, P. D., and Hodzic, D. (2006). Coupling of the nucleus and cytoplasm: role of the LINC complex. *J Cell Biol* **172,** 41-53.
12. Broers, J. L., Peeters, E. A., Kuijpers, H. J., Endert, J., Bouten, C. V., Oomens, C. W., Baaijens, F. P., and Ramaekers, F. C. (2004). Decreased mechanical stiffness in LMNA-/- cells is caused by defective nucleo-cytoskeletal integrity: implications for the development of laminopathies. *Hum Mol Genet* **13,** 2567-80.
13. Wilhelmsen, K., Litjens, S. H., Kuikman, I., Tshimbalanga, N., Janssen, H., van den Bout, I., Raymond, K., and Sonnenberg, A. (2005). Nesprin-3, a novel outer nuclear membrane protein, associates with the cytoskeletal linker protein plectin. *J Cell Biol* **171,** 799-810.
14. Ketema, M., Wilhelmsen, K., Kuikman, I., Janssen, H., Hodzic, D., and Sonnenberg, A. (2007). Requirements for the localization of nesprin-3 at the nuclear envelope and its interaction with plectin. *J Cell Sci* **120,** 3384-94.
15. Wilson, K. L. (2000). The nuclear envelope, muscular dystrophy and gene expression. *Trends Cell Biol* **10,** 125-9.
16. Bakay, M., Wang, Z., Melcon, G., Schiltz, L., Xuan, J., Zhao, P., Sartorelli, V., Seo, J., Pegoraro, E., Angelini, C., Shneiderman, B., Escolar, D., Chen, Y. W., Winokur, S. T., Pachman, L. M., Fan, C., Mandler, R., Nevo, Y., Gordon, E., Zhu, Y., Dong, Y., Wang, Y., and Hoffman, E. P. (2006). Nuclear envelope dystrophies show a transcriptional fingerprint suggesting disruption of Rb-MyoD pathways in muscle regeneration. *Brain* **129,** 996-1013.
17. Melcon, G., Kozlov, S., Cutler, D. A., Sullivan, T., Hernandez, L., Zhao, P., Mitchell, S., Nader, G., Bakay, M., Rottman, J. N., Hoffman, E. P., and Stewart, C. L. (2006). Loss of emerin at the nuclear envelope disrupts the Rb1/E2F and MyoD pathways during muscle regeneration. *Hum Mol Genet* **15,** 637-51.
18. Muchir, A., Pavlidis, P., Decostre, V., Herron, A. J., Arimura, T., Bonne, G., and Worman, H. J. (2007). Activation of MAPK pathways links LMNA mutations to cardiomyopathy in Emery-Dreifuss muscular dystrophy. *J Clin Invest* **117,** 1282-93.
19. Muchir, A., Pavlidis, P., Bonne, G., Hayashi, Y. K., and Worman, H. J. (2007). Activation of MAPK in hearts of EMD null mice: similarities between mouse models of X-linked and autosomal dominant Emery Dreifuss muscular dystrophy. *Hum Mol Genet* **16,** 1884-95.
20. Petrich, B. G., Gong, X., Lerner, D. L., Wang, X., Brown, J. H., Saffitz, J. E., and Wang, Y. (2002). c-Jun N-terminal kinase activation mediates downregulation of connexin43 in cardiomyocytes. *Circ Res* **91,** 640-7.
21. Petrich, B. G., Molkentin, J. D., and Wang, Y. (2003). Temporal activation of c-Jun N-terminal kinase in adult transgenic heart via cre-loxP-mediated DNA recombination. *Faseb J* **17,** 749-51.
22. Lee, J. S., Hale, C. M., Panorchan, P., Khatau, S. B., George, J. P., Tseng, Y., Stewart, C. L., Hodzic, D., and Wirtz, D. (2007). Nuclear lamin A/C deficiency induces defects in cell mechanics, polarization, and migration. *Biophys J* **93,** 2542-52.
23. Hale, C. M., Shrestha, A. L., Khatau, S. B., Stewart-Hutchinson, P. J., Hernandez, L., Stewart, C. L., Hodzic, D., and Wirtz, D. (2008). Dysfunctional connections between the nucleus and the actin and microtubule networks in laminopathic models. *Biophys J* **95,** 5462-75.

24. Houben, F., Willems, C. H., Declercq, I. L., Hochstenbach, K., Kamps, M. A., Snoeckx, L. H., Ramaekers, F. C., and Broers, J. L. (2009). Disturbed nuclear orientation and cellular migration in A-type lamin deficient cells. *Biochim Biophys Acta* **1793,** 312-24.
25. Piercy, R. J., Zhou, H., Feng, L., Pombo, A., Muntoni, F., and Brown, S. C. (2007). Desmin immunolocalisation in autosomal dominant Emery-Dreifuss muscular dystrophy. *Neuromuscul Disord* **17,** 297-305.
26. Nikolova, V., Leimena, C., McMahon, A. C., Tan, J. C., Chandar, S., Jogia, D., Kesteven, S. H., Michalicek, J., Otway, R., Verheyen, F., Rainer, S., Stewart, C. L., Martin, D., Feneley, M. P., and Fatkin, D. (2004). Defects in nuclear structure and function promote dilated cardiomyopathy in lamin A/C-deficient mice. *J Clin Invest* **113,** 357-69.
27. Muchir, A., Medioni, J., Laluc, M., Massart, C., Arimura, T., van der Kooi, A. J., Desguerre, I., Mayer, M., Ferrer, X., Briault, S., Hirano, M., Worman, H. J., Mallet, A., Wehnert, M., Schwartz, K., and Bonne, G. (2004). Nuclear envelope alterations in fibroblasts from patients with muscular dystrophy, cardiomyopathy, and partial lipodystrophy carrying lamin A/C gene mutations. *Muscle Nerve* **30,** 444-50.
28. Bonne, G., Mercuri, E., Muchir, A., Urtizberea, A., Becane, H. M., Recan, D., Merlini, L., Wehnert, M., Boor, R., Reuner, U., Vorgerd, M., Wicklein, E. M., Eymard, B., Duboc, D., Penisson-Besnier, I., Cuisset, J. M., Ferrer, X., Desguerre, I., Lacombe, D., Bushby, K., Pollitt, C., Toniolo, D., Fardeau, M., Schwartz, K., and Muntoni, F. (2000). Clinical and molecular genetic spectrum of autosomal dominant Emery-Dreifuss muscular dystrophy due to mutations of the lamin A/C gene. *Ann Neurol* **48,** 170-80.
29. Mittelbronn, M., Hanisch, F., Gleichmann, M., Stotter, M., Korinthenberg, R., Wehnert, M., Bonne, G., Rudnik-Schoneborn, S., and Bornemann, A. (2006). Myofiber degeneration in autosomal dominant Emery-Dreifuss muscular dystrophy (AD-EDMD) (LGMD1B). *Brain Pathol* **16,** 266-72.
30. Muchir, A., Bonne, G., van der Kooi, A. J., van Meegen, M., Baas, F., Bolhuis, P. A., de Visser, M., and Schwartz, K. (2000). Identification of mutations in the gene encoding lamins A/C in autosomal dominant limb girdle muscular dystrophy with atrioventricular conduction disturbances (LGMD1B). *Hum Mol Genet* **9,** 1453-9.
31. Rudnik-Schoneborn, S., Botzenhart, E., Eggermann, T., Senderek, J., Schoser, B. G., Schroder, R., Wehnert, M., Wirth, B., and Zerres, K. (2007). Mutations of the LMNA gene can mimic autosomal dominant proximal spinal muscular atrophy. *Neurogenetics* **8,** 137-42.
32. Charniot, J. C., Pascal, C., Bouchier, C., Sebillon, P., Salama, J., Duboscq-Bidot, L., Peuchmaurd, M., Desnos, M., Artigou, J. Y., and Komajda, M. (2003). Functional consequences of an LMNA mutation associated with a new cardiac and non-cardiac phenotype. *Hum Mutat* **21,** 473-81.
33. Perrot, A., Sigusch, H. H., Nagele, H., Genschel, J., Lehmkuhl, H., Hetzer, R., Geier, C., Leon Perez, V., Reinhard, D., Dietz, R., Josef Osterziel, K., and Schmidt, H. H. (2006). Genetic and phenotypic analysis of dilated cardiomyopathy with conduction system disease: demand for strategies in the management of presymptomatic lamin A/C mutant carriers. *Eur J Heart Fail* **8,** 484-93.
34. Fairley, E. A., Kendrick-Jones, J., and Ellis, J. A. (1999). The Emery-Dreifuss muscular dystrophy phenotype arises from aberrant targeting and binding of emerin at the inner nuclear membrane. *J Cell Sci* **112 (Pt 15),** 2571-82.
35. Motsch, I., Kaluarachchi, M., Emerson, L. J., Brown, C. A., Brown, S. C., Dabauvalle, M. C., and Ellis, J. A. (2005). Lamins A and C are differentially dysfunctional in autosomal dominant Emery-Dreifuss muscular dystrophy. *Eur J Cell Biol* **84,** 765-81.
36. Dimri, G. P., Lee, X., Basile, G., Acosta, M., Scott, G., Roskelley, C., Medrano, E. E., Linskens, M., Rubelj, I., Pereira-Smith, O., and et al. (1995). A biomarker that identifies

senescent human cells in culture and in aging skin in vivo. *Proc Natl Acad Sci U S A* **92,** 9363-7.

37. Ellis, J. A., Craxton, M., Yates, J. R., and Kendrick-Jones, J. (1998). Aberrant intracellular targeting and cell cycle-dependent phosphorylation of emerin contribute to the Emery-Dreifuss muscular dystrophy phenotype. *J Cell Sci* **111 (Pt 6),** 781-92.
38. Geary, S. M., Cowin, A. J., Copeland, B., Baleato, R. M., Miyazaki, K., and Ashman, L. K. (2008). The role of the tetraspanin CD151 in primary keratinocyte and fibroblast functions: implications for wound healing. *Exp Cell Res* **314,** 2165-75.
39. Dunn, G. A., and Brown, A. F. (1986). Alignment of fibroblasts on grooved surfaces described by a simple geometric transformation. *J Cell Sci* **83,** 313-40.
40. Holt, M. R., Calle, Y., Sutton, D. H., Critchley, D. R., Jones, G. E., and Dunn, G. A. (2008). Quantifying cell-matrix adhesion dynamics in living cells using interference reflection microscopy. *J Microsc* **232,** 73-81.
41. Sakaki, M., Koike, H., Takahashi, N., Sasagawa, N., Tomioka, S., Arahata, K., and Ishiura, S. (2001). Interaction between emerin and nuclear lamins. *J Biochem (Tokyo)* **129,** 321-7.
42. Raharjo, W. H., Enarson, P., Sullivan, T., Stewart, C. L., and Burke, B. (2001). Nuclear envelope defects associated with LMNA mutations cause dilated cardiomyopathy and Emery-Dreifuss muscular dystrophy. *J Cell Sci* **114,** 4447-57.
43. Capanni, C., Cenni, V., Mattioli, E., Sabatelli, P., Ognibene, A., Columbaro, M., Parnaik, V. K., Wehnert, M., Maraldi, N. M., Squarzoni, S., and Lattanzi, G. (2003). Failure of lamin A/C to functionally assemble in R482L mutated familial partial lipodystrophy fibroblasts: altered intermolecular interaction with emerin and implications for gene transcription. *Exp Cell Res* **291,** 122-34.
44. Strelkov, S. V., Schumacher, J., Burkhard, P., Aebi, U., and Herrmann, H. (2004). Crystal structure of the human lamin A coil 2B dimer: implications for the head-to-tail association of nuclear lamins. *J Mol Biol* **343,** 1067-80.
45. Johnson, B. R., Nitta, R. T., Frock, R. L., Mounkes, L., Barbie, D. A., Stewart, C. L., Harlow, E., and Kennedy, B. K. (2004). A-type lamins regulate retinoblastoma protein function by promoting subnuclear localization and preventing proteasomal degradation. *Proc Natl Acad Sci U S A* **101,** 9677-82.
46. Van Berlo, J. H., Voncken, J. W., Kubben, N., Broers, J. L., Duisters, R., van Leeuwen, R. E., Crijns, H. J., Ramaekers, F. C., Hutchison, C. J., and Pinto, Y. M. (2005). A-type lamins are essential for TGF-beta1 induced PP2A to dephosphorylate transcription factors. *Hum Mol Genet* **14,** 2839-49.
47. Favreau, C., Higuet, D., Courvalin, J. C., and Buendia, B. (2004). Expression of a mutant lamin A that causes Emery-Dreifuss muscular dystrophy inhibits in vitro differentiation of C2C12 myoblasts. *Mol Cell Biol* **24,** 1481-92.
48. Muchir, A., van Engelen, B. G., Lammens, M., Mislow, J. M., McNally, E., Schwartz, K., and Bonne, G. (2003). Nuclear envelope alterations in fibroblasts from LGMD1B patients carrying nonsense Y259X heterozygous or homozygous mutation in lamin A/C gene. *Exp Cell Res* **291,** 352-62.
49. Pekovic, V., Harborth, J., Broers, J. L., Ramaekers, F. C., van Engelen, B., Lammens, M., von Zglinicki, T., Foisner, R., Hutchison, C., and Markiewicz, E. (2007). Nucleoplasmic LAP2alpha-lamin A complexes are required to maintain a proliferative state in human fibroblasts. *J Cell Biol* **176,** 163-72.
50. Sasseville, A. M., and Langelier, Y. (1998). In vitro interaction of the carboxy-terminal domain of lamin A with actin. *FEBS Lett* **425,** 485-9.
51. Kornberg, L., Earp, H. S., Parsons, J. T., Schaller, M., and Juliano, R. L. (1992). Cell adhesion or integrin clustering increases phosphorylation of a focal adhesion-associated tyrosine kinase. *J Biol Chem* **267,** 23439-42.

52. Yujiri, T., Ware, M., Widmann, C., Oyer, R., Russell, D., Chan, E., Zaitsu, Y., Clarke, P., Tyler, K., Oka, Y., Fanger, G. R., Henson, P., and Johnson, G. L. (2000). MEK kinase 1 gene disruption alters cell migration and c-Jun NH2-terminal kinase regulation but does not cause a measurable defect in NF-kappa B activation. *Proc Natl Acad Sci U S A* **97,** 7272-7.
53. Muchir, A., Wu, W., and Worman, H. J. (2009). Reduced expression of A-type lamins and emerin activates extracellular signal-regulated kinase in cultured cells. *Biochim Biophys Acta* **1792,** 75-81.
54. Goldman, R. D., Shumaker, D. K., Erdos, M. R., Eriksson, M., Goldman, A. E., Gordon, L. B., Gruenbaum, Y., Khuon, S., Mendez, M., Varga, R., and Collins, F. S. (2004). Accumulation of mutant lamin A causes progressive changes in nuclear architecture in Hutchinson-Gilford progeria syndrome. *Proc Natl Acad Sci U S A* **101,** 8963-8.
55. Fairley, E. A., Riddell, A., Ellis, J. A., and Kendrick-Jones, J. (2002). The cell cycle dependent mislocalisation of emerin may contribute to the Emery-Dreifuss muscular dystrophy phenotype. *J Cell Sci* **115,** 341-54.
56. Chen, Q., Kinch, M. S., Lin, T. H., Burridge, K., and Juliano, R. L. (1994). Integrin-mediated cell adhesion activates mitogen-activated protein kinases. *J Biol Chem* **269,** 26602-5.
57. Zhu, X., and Assoian, R. K. (1995). Integrin-dependent activation of MAP kinase: a link to shape-dependent cell proliferation. *Mol Biol Cell* **6,** 273-82.
58. Fincham, V. J., James, M., Frame, M. C., and Winder, S. J. (2000). Active ERK/MAP kinase is targeted to newly forming cell-matrix adhesions by integrin engagement and v-Src. *Embo J* **19,** 2911-23.
59. Ishibe, S., Joly, D., Liu, Z. X., and Cantley, L. G. (2004). Paxillin serves as an ERK-regulated scaffold for coordinating FAK and Rac activation in epithelial morphogenesis. *Mol Cell* **16,** 257-67.
60. Klemke, R. L., Cai, S., Giannini, A. L., Gallagher, P. J., de Lanerolle, P., and Cheresh, D. A. (1997). Regulation of cell motility by mitogen-activated protein kinase. *J Cell Biol* **137,** 481-92.
61. Discher, D. E., Janmey, P., and Wang, Y. L. (2005). Tissue cells feel and respond to the stiffness of their substrate. *Science* **310,** 1139-43.
62. Gonzalez, J. M., Navarro-Puche, A., Casar, B., Crespo, P., and Andres, V. (2008). Fast regulation of AP-1 activity through interaction of lamin A/C, ERK1/2, and c-Fos at the nuclear envelope. *J Cell Biol* **183,** 653-66.
63. Rodriguez-Viciana, P., Tetsu, O., Tidyman, W. E., Estep, A. L., Conger, B. A., Cruz, M. S., McCormick, F., and Rauen, K. A. (2006). Germline mutations in genes within the MAPK pathway cause cardio-facio-cutaneous syndrome. *Science* **311,** 1287-90.

**Acknowledgements**

LJE was funded by the Muscular Dystrophy Campaign (Grant number RA3/655) awarded to JAE. MW was supported by a grant from the German Network of Muscular Dystrophies (MD-NET, 01GM0302) funded by the German ministry of education and research (BMBF) and an EU grant Euro-Laminopathies contract #018690.

Table 1.

Mean persistence and speed values from the scratch and cell motility assays.

| | **WT6000** | **R401C** |
|---|---|---|
| **Scratch assay:** | n = 33 | n = 39 |
| Mean persistence | 0.62 ± 0.057 | 0.62 ± 0.05<br>$p < 0.01$ |
| Mean speed | 10.57 ± 0.69 | 13.12 ± 0.75<br>$p < 0.02$ |
| **Cell motility assay:** | n = 65 | n = 50 |
| Mean persistence | 0.57 ± 0.065 | 0.56 ± 0.058<br>$p < 0.01$ |
| Mean speed | 6.89 ± 0.26 | 8.19 ± 0.40<br>$p < 0.02$ |

Figure 1

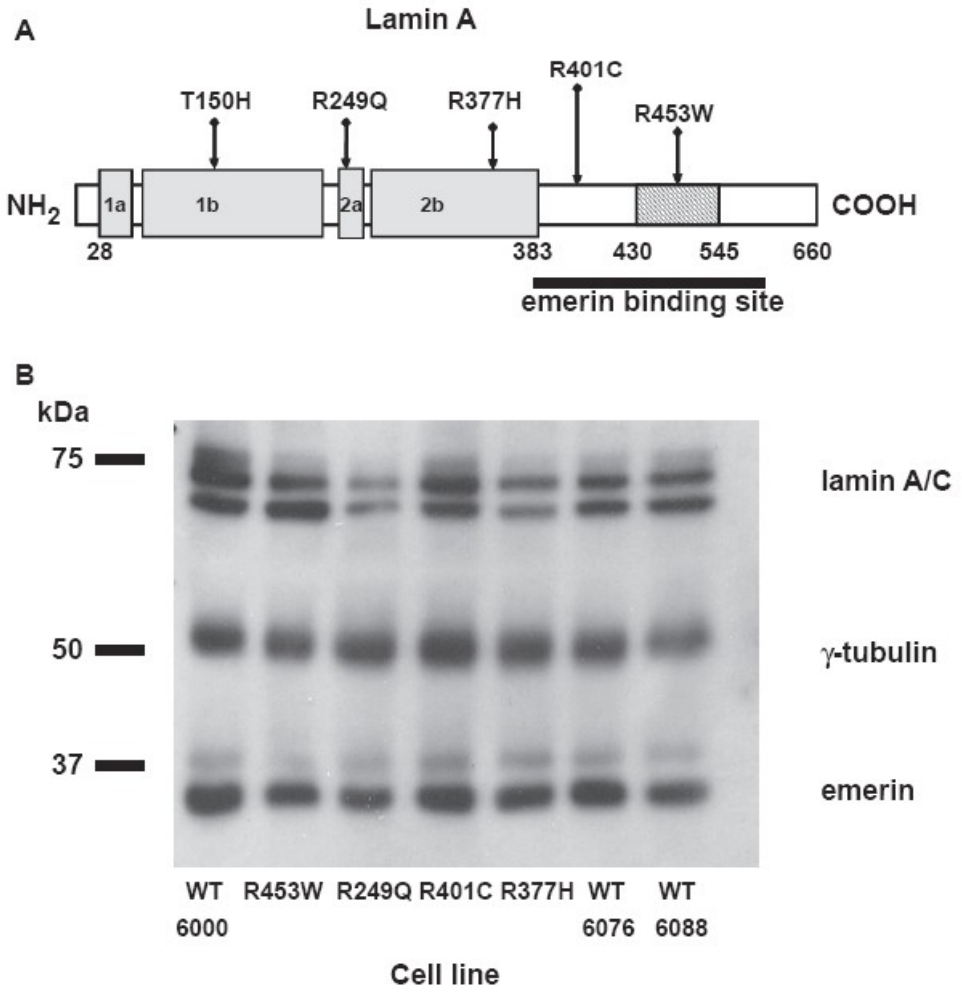
A
Lamin A
T150H
R249Q
R377H
R401C
R453W
NH2
1a
1b
2a
2b
COOH
28
383
430
545
660
emerin binding site
B
kDa
75
50
37
lamin A/C
γ-tubulin
emerin
WT 6000
R453W
R249Q
R401C
R377H
WT 6076
WT 6088
Cell line
C
S B S B S B S B S B S B
37
emerin
WT6000 R453W R249Q R401C R377H control
Cell line
D
% emerin bound to lamin A/C
60
50
40
30
20
10
0
WTav
R401C
R453W
R249Q
R377H
Cell line

Figure 2

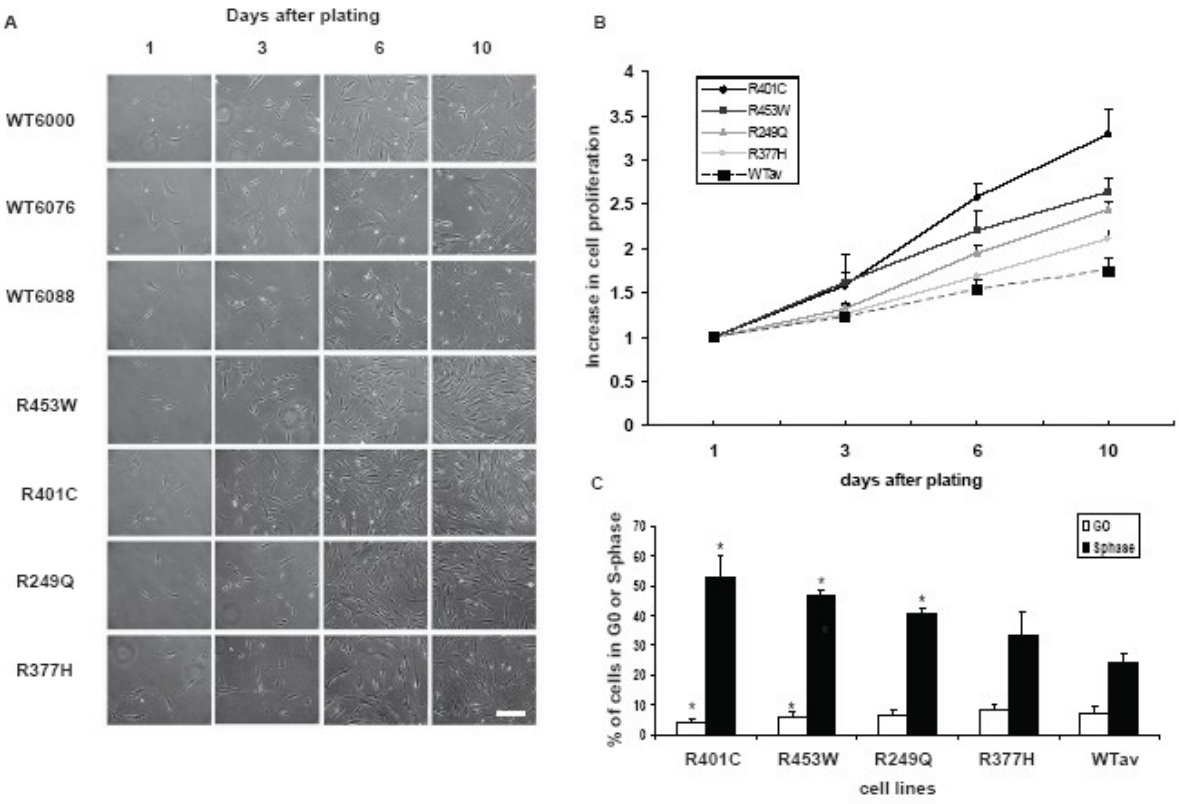

Figure 3

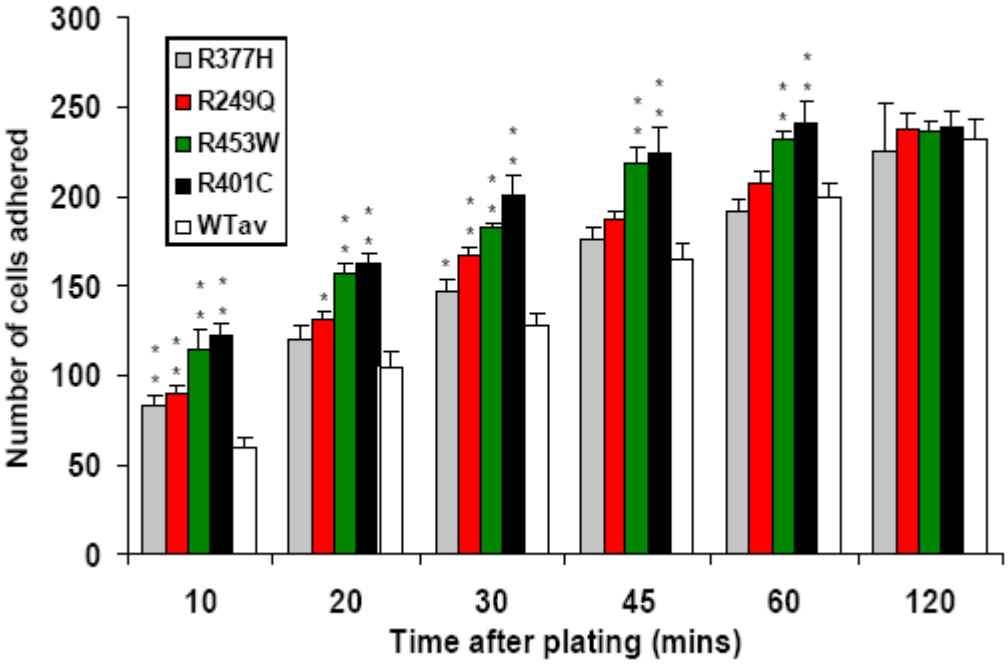

Figure 4

A

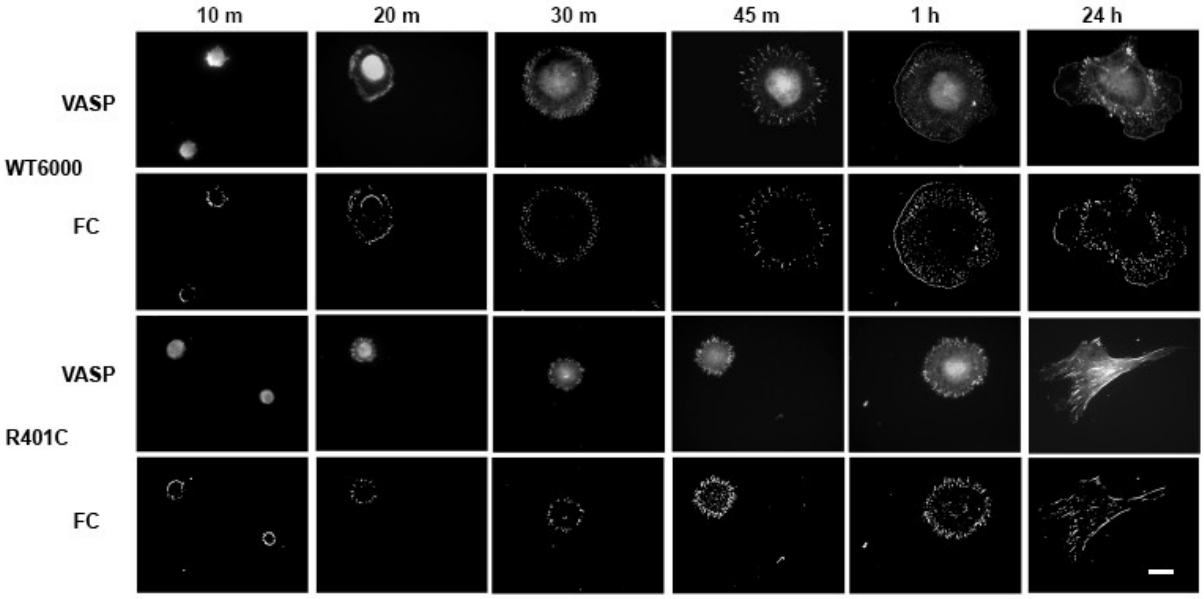

Figure 4

B

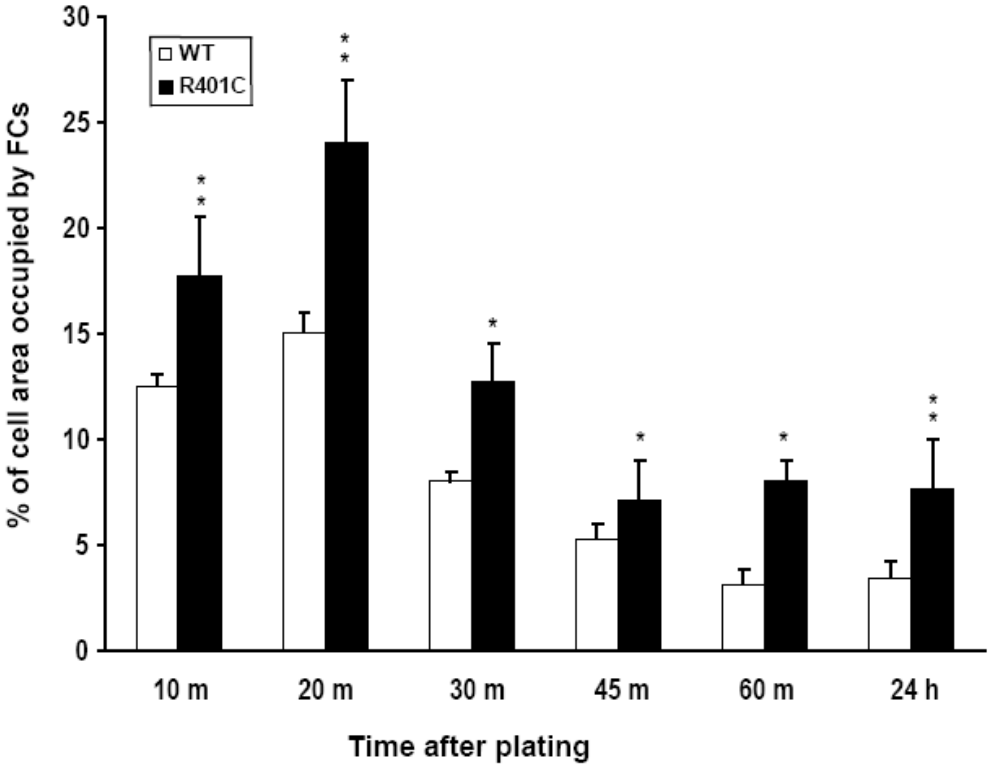


C

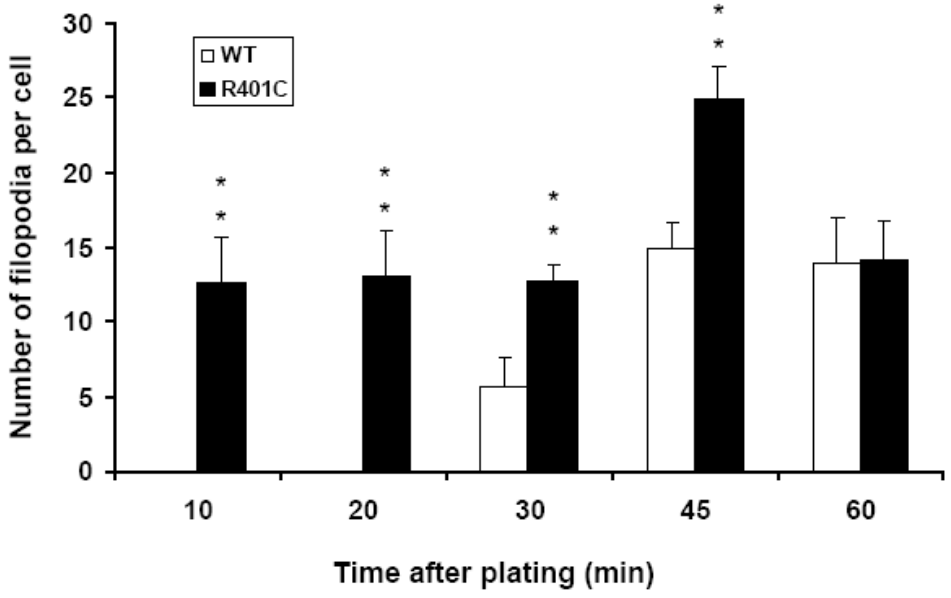

Figure 4

D

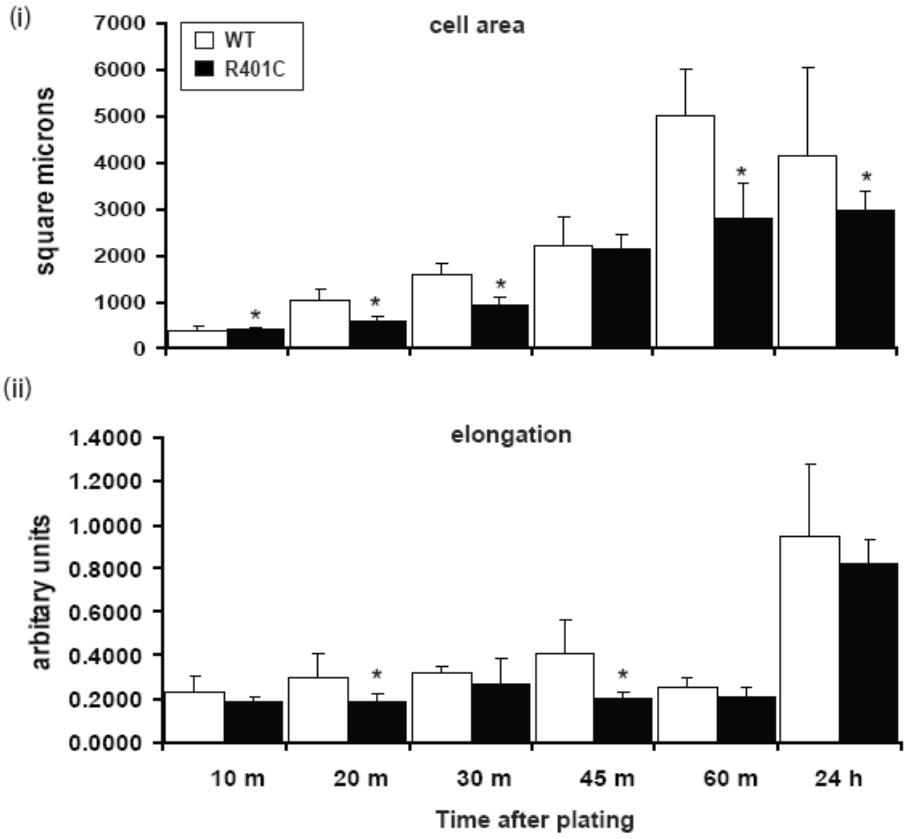

**Figure 5**

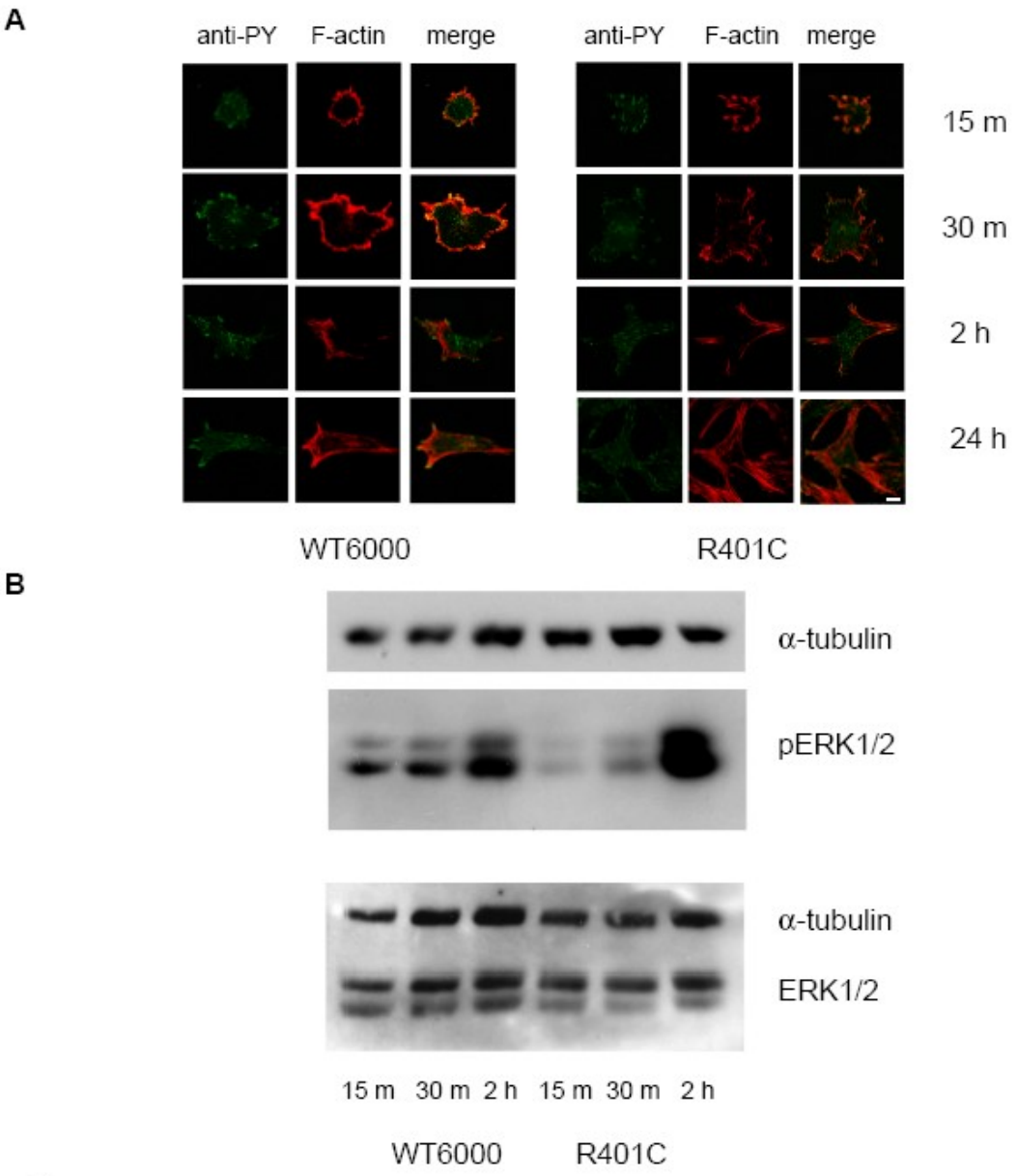

Figure 6